https://doi.org/10.1364/OL.412699

Photoconductive terahertz generation in semi-insulating GaAs and InP under the extremes of bias field and pump fluence

SALMAN ALFIHED[1,2], MATTHIAS F. JENNE[1], ANTONIA CIOCOIU[1], IAN G. FOULDS[1], AND JONATHAN F. HOLZMAN[1,*]

[1]School of Engineering, The University of British Columbia, 1137 Alumni Avenue, Kelowna, BC V1V 1V7, Canada
[2]Materials Science Research Institute, King Abdulaziz City for Science and Technology, Riyadh, 11442, Saudi Arabia
*Corresponding author: jonathan.holzman@ubc.ca

Received XX Month XXXX; revised XX Month, XXXX; accepted XX Month XXXX; posted XX Month XXXX (Doc. ID XXXXX); published XX Month XXXX

This work analyses photoconductive (PC) terahertz (THz) emitters based upon the semi-insulating (SI) forms of GaAs and InP. Dependencies of the emitters are studied under the extremes of bias field and pump fluence to reveal the underlying physics of charge carrier photoexcitation, transport, and emission. The bias field dependence shows that SI-GaAs PC THz emitters are preferentially subject to space-charge-limited current, under the influence of trap states, while SI-InP PC THz emitters are preferentially subject to sustained current, due to a prolonged charge carrier lifetime and the ensuing Joule heating. This leads to differing frontrunners for performance with respect to a critical bias field. The pump fluence dependence shows space-charge and near-field screening for all PC THz emitters, with SI-GaAs predisposed to near-field screening (under the influence of transient mobility) and SI-InP predisposed to space-charge screening. Such findings can support a deeper understanding on the underlying physics and optimal performance of SI-GaAs and SI-InP PC THz emitters. © 2020 Optical Society of America

Terahertz (THz) radiation occupies a distinct region of the electromagnetic spectrum—with frequencies (0.1 – 10 THz) that give it unique perspectives in applications. Terahertz spectroscopy benefits from the fact that THz radiation is nonionizing and resonant with many molecular modes [1,2]. Terahertz imaging leverages the penetrating properties of THz radiation in characterizing refraction and absorption as a function of space [3]. Terahertz communication applies the high carrier frequencies and coherence of THz radiation to wireless systems [4]. While most schemes for generating THz radiation can be classified as photoconductive(PC) emission [5,6] andoptical rectification [7,8], PC THz emission is particularly effective in generating high-power and broadband THz radiation—and it is the focus of this work.

The PC THz emitter incorporates a biased PC gap whose radiative emission is defined largely by its semiconductor. This has led to the development of PC THz emitters with InAs, InSb, InGaAs, GaSb [5], and other semiconductors, with especially keen interest on the semi-insulating (SI) materials SI-GaAs and SI-InP [6,9]. The high resistivities and mobilities of SI-GaAs and SI-InP have led to their widespread use in PC THz emitters—as well as a competition on their performance under the extremes of bias field and pump fluence [10].

In this work, the dynamics of PC THz emission in SI-GaAs and SI-InP are explored for a broad range of bias fields and pump fluences in the PC THz emitters—with key insights drawn from a generalized model of charge carrier photoexcitation, transport, and emission. The model considers bias field dependencies from space-charge limited current (as influenced by trap states) and sustained current (as a result of prolonged charge carrier lifetimes and seen through Joule heating), as well as pump fluence dependencies from space-charge and near-field screening (with transient mobility). We hypothesize that the SI-GaAs PC THz emitters will be preferentially subject to space-charge-limited current, given SI-GaAs's prominent trap states [11,12], and the SI-InP PC THz emitters will be preferentially subject to sustained current, due to SI-InP's prolonged charge carrier lifetime and propensity for Joule heating [9,13]. We also expect the SI-GaAs and SI-InP PC THz emitters to exhibit saturation with respect to the pump fluence, although the levels of space-charge and near-field screening will likely differ. The generalized model is used to characterize these dynamics and test our hypotheses—foradeeperunderstandingontheunderlyingphysicsand optimal performance of SI-GaAs and SI-InP PC THz emitters.

The model applied in this work considers a PC THz emitter having a biased PC gap, as shown in Fig. 1, with dimensions of L_x and L_y along its x-axis and y-axis, respectively. The x-axis (parallel to the bias field) and y-axis (perpendicular to the bias field) are in the plane of the PC gap; the z-axis is normal to the PC gap (parallel to the radiative emission). It is photoexcited by an ultrashort pump pulse with an intensity of $I_p(x,t) = 2(\ln(2)/\pi)^{½} \cdot \Phi_p/\tau_d \cdot \exp(-4\ln(2)(t^2/\tau_d^2 + x^2/x_d^2))$, where Φ_p is the pump fluence, in μJ/cm^2, τ_d is the pump pulse duration, as a full-width-at-half-maximum, and x_d is the pump pulse diameter, as a full-width-at-half-maximum. The photoexcited charge carriers accelerate in the bias field, E_b, which is assumed to be uniform across the PC gap, yielding a surface current density of $k_s(x,t)$, in A/cm, and a far-field THz pulse with an electric field, at a distance z and time t, of [10,14,15]

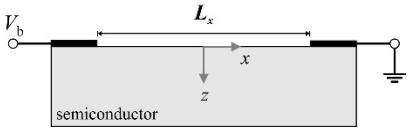

Fig. 1. The PC gap with a length of L_x and bias voltage of V_b, giving a bias field parallel to the x-axis and PC THz emission parallel to the z-axis.

$$E_{\mathrm{THz}}(z,t) = \frac{L_y}{4\pi\varepsilon_0 c^2 z}\frac{d}{dt}\int_{-L_x/2}^{+L_x/2} k_s(x,t)dx\,, \qquad (1)$$

where ε_0 is the permittivity of free space and c is the free-space speed of light. In this work, the strength of a far-field THz pulse is defined by a peak-to-peak THz field amplitude of E_{THz}. At low bias fields and pump fluences, the surface current density, $k_s(x,t)$, and THz field amplitude, E_{THz}, scale in a simple linear manner with respect to the bias field, E_b, and pump fluence, Φ_p. However, nonlinearities can arise at higher bias fields and pump fluences. The nonlinearities can be characterized by rate equations that govern the electron surface charge density, $n_s(x,t)$, and hole surface charge density, $p_s(x,t)$, both in cm^{-2}, via [10,14,15]

$$\frac{\partial n_s(x,t)}{\partial t} \approx \frac{(1-R)\Phi_p}{\tau_d h\nu}\exp\left(-4\ln 2\left(\frac{t^2}{\tau_d^2}+\frac{x^2}{x_d^2}\right)\right)+\frac{1}{q_e}\frac{\partial k_s(x,t)}{\partial x}, \qquad (2a)$$

$$\frac{\partial p_s(x,t)}{\partial t} \approx \frac{(1-R)\Phi_p}{\tau_d h\nu}\exp\left(-4\ln 2\left(\frac{t^2}{\tau_d^2}+\frac{x^2}{x_d^2}\right)\right), \qquad (2b)$$

respectively. Here, $R = (1 - \varepsilon_r^{1/2})^2/(1 + \varepsilon_r^{1/2})^2$ is the reflectivity of the air-semiconductor surface with a dielectric constant of $\varepsilon_r \approx 12.8$ for SI-GaAs and $\varepsilon_r \approx 12.5$ for SI-InP, h is Planck's constant, ν is the frequency of the pump photons, and q_e is the electronic charge. It is assumed here that charge carrier diffusion is negligible, which is reasonable over the picosecond duration of THz radiative emission, and that the hole mobility is far less than the electron mobility, which we deem to be acceptable for SI-GaAs and SI-InP. Such assumptions allow the surface current density, $k_s(x,t)$, to be linked to electron transport, by Eq. (2a), leaving a surface charge density for the immobile holes of $p_s(x,t) = (\pi/\ln(2))^{1/2}(1 - R)\,\Phi_p/(4\,h\nu)\cdot(1 + \mathrm{erf}(2(\ln(2))^{1/2}t/\tau_d))\cdot\exp(-4\ln(2)x^2/x_d^2)$, from Eq. (2b). The THz field amplitude, E_{THz}, is then defined from the surface charge density, $k_s(x,t)$, by way of Eq. (1).

Nonlinearities in the THz field amplitude, E_{THz}, with respect to the bias field, E_b, are revealed in two opposing forms. Superlinearity can arise from space-charge-limited current with its level impacted by trap states. Both SI-GaAs [12,16] and SI-InP [17] can show this nonlinearity, but SI-GaAs is especially susceptible to the effects of trap states due to its deep EL2 traps [18]. Sublinearity can arise from sustained current, which leads to Joule heating and is of concern in semiconductors with long charge carrier lifetimes [19,20]. (The energy dissipated by Joule heating is proportional to the duration of photocurrent flow and is thus set by the charge carrier lifetime [9].) This spurred attempts to reduce charge carrier lifetimes and lessen Joule heating in both SI-GaAs [19] and SI-InP [9]. Such superlinearity and sublinearity are characterized in this work by a term having a generalized exponent in the (otherwise linear) relation for surface current density, $k_s(x,t)$, and electric field distribution, $E(x,t)$, in the PC gap. Thus, $k_s(x,t)$ is made proportional to $E(x,t)(1 + (E(x,t)/E_{\mathrm{ref}})^{\beta})/2$, with β as the fitted exponent and E_{ref} as the fitted reference bias field. Such a relation can capture the linearity seen in saturates the THz field amplitude at high charge carrier densities. It evolves in the PC gap according to Poisson's equation, which relates the electric field distribution, $E(x,t)$, to the electron and hole surface charge densities via [14,15]

$$\frac{\partial E(x,t)}{\partial x} = \frac{q_e}{\varepsilon_r\varepsilon_0\delta_d}\left(p_s(x,t) - n_s(x,t)\right), \qquad (3)$$

where $\delta_d = 0.74$ μm and 0.33 μm are the pump pulse's penetration depths in SI-GaAs and SI-InP, respectively. Near-field screening has the THz near-field in the PC gap oppose the bias field, which also saturates the THz field amplitude at high charge carrier densities. It is defined by matching fields as boundary conditions at the air-semiconductor interface, which gives a surface current density of [10,14,15]

$$k_n(x,t) = \left(\frac{q_e\,\mu_n(\Phi_p)\,n_s(x,t)}{1 + g_{\mathrm{NF}}\,q_e\,\eta_0\left(1+\sqrt{\varepsilon_r}\right)^{-1}\mu_n(\Phi_p)\,n_s(x,t)}\right) \times E(x,t)\left(1 + (E(x,t)/E_{\mathrm{ref}})^{\beta}\right)/2, \qquad (4)$$

where η_0 is the impedance of free space. We see near-field screening arise here as a saturation of the surface current density, $k_s(x,t)$, and thus the THz field amplitude, E_{THz}, when the electron surface charge density, $n_s(x,t)$, drives the denominator's second term towards unity. The above expression differs from those of prior works [10,14,15] in that it encompasses nonlinearities with respect to the bias field, via the parameters β and E_{ref}, and perturbations from a semi-infinite (large-aperture) structure, via the dimensionless near-field control parameter g_{NF}. This g_{NF} is a fitting parameter that is near unity for large-aperture PC THz emitters and less for smaller PC THz emitters. The above expression also includes a pump-fluence-dependent electron mobility, $\mu_n(\Phi_p)$, to recognize that large pump fluences can form dense electron-hole plasmas with increased scattering rates between the (typically hot) charge carriers [21]. This can drastically reduce the mobility over the picosecond duration of THz radiative emission. This electron mobility is cast in the form of the Caughey-Thomas relation [22],

$$\mu_n(\Phi_p) = \left(\frac{\mu_{\max} - \mu_{\min}}{1 + (\Phi_p/\Phi_{\mathrm{ref}})^{\alpha}} + \mu_{\min}\right), \qquad (5)$$

prior works with $\beta = 0$ [10,14,15], while encompassing space-charge-limited current with $\beta > 0$ or sustained current with $\beta < 0$.

Nonlinearities in the THz field amplitude, E_{THz}, with respect to the pump fluence, Φ_p, are revealed through space-charge screening and/or near-field screening. Space-charge screening has the polarizing electrons and holes form a space-charge field that opposes the bias field, which

populated by the values of Table I in [23]. For SI-GaAs and SI-InP, the maximum mobilities are μ_{max} = 9,400 cm^2/(V·s) and 5,200 cm^2/(V·s), the minimum mobilities are μ_{min}= 500 cm^2/(V·s) and 400 cm^2/(V·s), thereference pump fluences are Φ_{ref} = 0.58 μJ/cm^2 and 1.2 μJ/cm^2, and theexponential factors are α = 0.394 and 0.470, respectively.

Overall, theabovegeneralizedmodelisappliedforasetbias field, E_b, and pump fluence, Φ_p, by solving for the hole surface charge density, $p_s(x,t)$, electron surface charge density, $n_s(x,t)$, electric field distribution, $E(x,t)$, and surface current density, $k_s(x,t)$, across the PC gap using Eqs. (2) – (4), with the electron mobility, $\mu_n(\Phi_p)$, defined by Eq. (5). The surface current density, $k_s(x,t)$, is then used in Eq. (1) to determine the peak-to- peak THz field amplitude, E_{THz}.

The PC THz emitters incorporate features with 25-nm/75-nm Cr/Au metallization on high-resistivity Cr-doped SI-GaAs and Fe-doped SI-InP. The PCgapstake theform of 10-μm-wide striplines separated by PC gap lengths of L_x = 100, 200, and 300 μm. (Striplines are used here to applya sufficiently uniform bias field, as assumed by the model.) The PC THz emitters were tested in a THz time-domain-spectroscopy system with the bias voltage, V_b, and pump power, P_p, varied to apply the desired bias field, E_b, and pump fluence, Φ_p, respectively. The system used an ultrafast pulsed laser (Spectra Physics-Mai Tai HP) with a pump pulse duration of τ_p = 70 fs, repetition rate of 80 MHz, and wavelength of 800nm, giving a 1.55-eV photon energy that is above the 1.43 eV bandgap of SI-GaAs and the 1.34 eV bandgap of SI-InP.

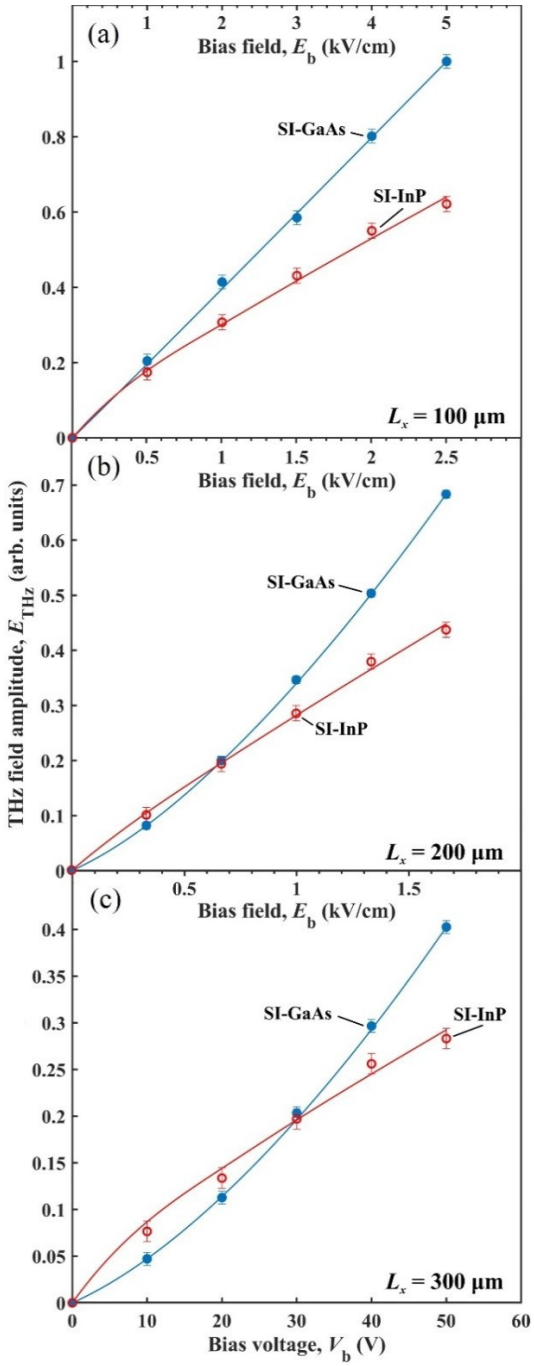

Fig. 2. Terahertz field amplitude, E_{THz}, versus peak-to-peak bias voltage, V_b, on the lower axis and peak-to-peak bias field, E_b, on the elevated axes. Subplots (a), (b), and (c) apply to PC gap lengths of L_x = 100, 200, and 300 μm, pump spot diameters of x_p = 75, 190, and 290 μm, and pump fluences of Φ_p = 113.2, 17.6, and 7.57 μJ/cm^2, respectively, at a set pump power of P_p = 0.4 W. Experimental data and theoretical (best-fit) curves are shown for SI-GaAs PC THz emitters as solid blue circles and solid blue lines, respectively, and SI-InP PC THz emitters as hollow red circles and solid red lines, respectively.

Figures 2(a), (b), and (c) show experimental and theoretical results for THz field amplitude, E_{THz}, versus peak-to-peak bias voltage, V_b, on the lower axis and peak-to-peak bias field, E_b, on the elevated axes for PC gap lengths of L_x =100, 200, and 300 μm, pump spot diameters of x_p = 75, 190, and 290 μm, and pump fluences of Φ_p = 113.2, 17.6, and 7.57 μJ/cm^2, respectively, at a set pump power of P_p = 0.4 W. Experimental data and theoretical curves are displayed for the SI-GaAs PC THz emitters as solid blue circles and solid blue lines, respectively, and the SI-InP PC THz emitters as hollow red circles and solid red lines, respectively. The theoretical curves in the three plots are best fits with parameter values giving mean percentage errors of 0.88%, 0.41%, and 1.7%, respectively. It is apparent from the overall results that the manner in which the THz field amplitude, E_{THz}, rises with respect to the bias field, E_b, differs for the two semiconductors. In Figs. 2(a), (b), and (c) superlinear curves are seen for the SI-GaAs PC THz emitters, with β = +0.02, +0.61, and +0.74 and E_{ref} = 0.74, 0.96, and 1.0 kV/cm, respectively, and sublinear curves are seen for the SI-InP PC THz emitters, with β = –0.62, –0.2, and –0.46 and E_{ref} = 0.74, 0.96, and 1.0 kV/cm, respectively. The positive β values for the SI-GaAs PC THz emitters suggest that they are preferentially subject to space-charge-limited current. This would manifest as quadratic dependence on the bias field (β = 1) according to the Mott-Gurney relation, for no influence from trap states [24], and so the sub-quadratic dependence (β < 1) seen here suggests that trap states play a role. This is reasonable given the deep EL2 traps in SI-GaAs's bandgap and prior current-voltage characterizations of SI-GaAs showing sub-quadratic dependencies associated to trap states [11]. The negative β values for the SI-InP PC THz emitters suggest that they are subject to sustained current, and heightened Joule heating, from a prolonged charge carrier lifetime. Such a finding agrees with our prior pump-probe studies of SI-InP, showing sustained (nanosecond-duration) charge carrier lifetimes [13], and our studies of SI-InP PC THz emitters, for which surface states play a critical role in the charge carriers' cooling and recombination [9]. Overall, the superlinear and sublinear trends for the PC THz emitters yield a low-field regime, with SI-InP outperforming SI-GaAs, and a high-field regime, with SI-GaAs outperforming SI-InP. The regimes are delineated in Figs. 2(a), (b), and (c) by bias voltages of V_b=9.3, 19.5, and 29.5 V, respectively, at a critical bias field, $E_b \approx 0.96$ kV/cm, where the SI-GaAs and SI-InP PC THz emitters yield equal THz field amplitudes. Below this critical bias field, the penalties of space-charge-limited current in SI-GaAs outweigh the penalties of sustained current in SI-InP, while the opposite weighting is seen above this critical bias field.

Figures 3(a), (b), and (c) show results for THz field amplitude, E_{THz}, versus pump power, P_p, on the lower axis and pump fluence, Φ_b, on the elevated axes for PC gaplengths of L_x = 100, 200, and 300 μm, pump spot diameters of x_p = 75, 190, and 290 μm, and peak-to-peak bias fields of E_b = 4.0, 2.0, and 1.4 kV/cm, respectively, given a set peak-to-peak bias voltage of V_b = 40 V. Experimental data and theoretical curves are displayed for the SI-GaAs PC THz emitters as solid blue circles and solid blue lines, respectively, and for the SI-InP PC THz emitters as hollow red circles and solid red lines, respectively. The theoretical curves in the three plots are best fits with parameter values giving mean percentage errors of 2.6%, 1.2%, and 2.0%, respectively. All PC THz emitters show a sublinear rise in THz field amplitude, E_{THz}, as the pump fluence, Φ_p, increases and screening arises. The space-charge and near-field screeningcan beidentifiedby theparametervalues. Forthe SI-GaAs and SI-InP PC THz emitters, the near-field control parameters are g_{NF} = 0.054 and 0.026 for L_x = 100 μm, g_{NF} = 0.19 and 0.030 for L_x = 200 μm, and g_{NF} = 0.38 and 0.032 for L_x = 300 μm, respectively. The greater g_{NF} values for the SI-GaAs PC THz emitters indicate that they are more susceptible to near-field screening. This is logical as the penetration depth, δ_i, of SI-GaAs is roughly twice that of SI-InP, which halves the space-charge field in Eq. (3) and weakens the space-charge screening. We also see that the g_{NF} values grow along with the PC gap length L_x. We attribute this growth in g_{NF} to the lengthening PC gap, which has the emitters transition towards the semi-infinite (large-aperture) structure that is assumed in Eq. (4).

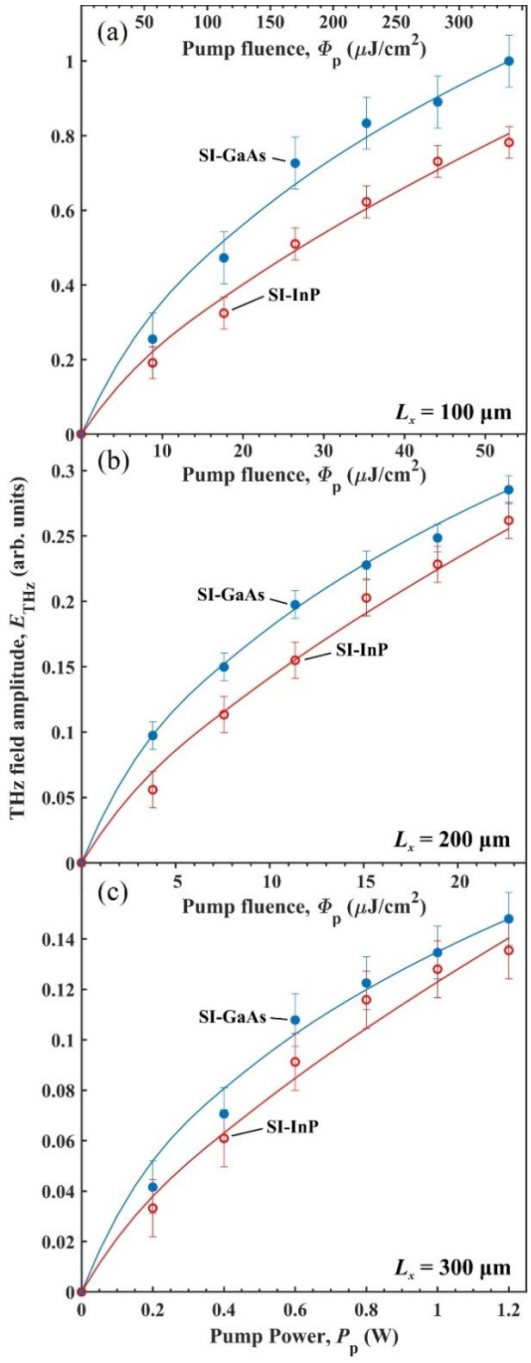

Fig. 3. Terahertz field amplitude, E_{THz}, versus pump power, P_p, on the lower axis and pump fluence, Φ_p, on the elevated axes. Subplots (a), (b), and (c) apply to PC gap lengths of L_x = 100, 200, and 300 µm, pump spot diameters of x_p = 75, 190, and 290 µm, and peak-to-peak bias fields of E_b = 4.0, 2.0, and 1.4 kV/cm, respectively, at a set peak-to-peak bias voltage of V_b = 40 V. Experimental data and theoretical (best-fit) curves are displayed for SI-GaAs PC THz emitters as solid blue circles and solid blue lines, respectively, and SI-InP PC THz emitters as hollow red circles and solid red lines, respectively.

In this work, we analysed PC THz emitters based upon SI-GaAs and SI-InP and found varying dependencies under the extremes of bias field and pump fluence. The bias field dependence showed that SI-GaAs PC THz emitters are preferentially subject to space-charge-limited current, under the influence of trap states, and SI-InP PC THz emitters are preferentially subject to sustained current, due to a prolonged charge carrier lifetime and the ensuing Joule heating. This led to varying levels and differing frontrunners for the performance of SI-GaAs and SI-InP PC THz emitters with respect to a critical bias field. (While low-temperature-grown GaAs (LT-GaAs) was not studied here, we anticipate that its scaling with bias field and pump fluence would mimic that of SI-GaAs as its subpicosecond [5] charge carrier lifetime is less than SI-GaAs's picosecond lifetime [19] and far less than SI-InP's nanosecond lifetime [13].) The pump fluence dependence showed the presence of space-charge and near-field screening for all of the PC THz emitters, with those incorporating SI-GaAs and SI-InP being preferentially subject to near-field screening and space-charge screening, respectively. Ultimately, it is hoped that these findings will yield deeper understanding on the underlying physics of SI-GaAs and SI-InP PC THz emitters—and will foster their continuing development.

Funding. This work was supported in part by the Natural Sciences and Engineering Research Council of Canada (RGPIN-2015-06711 and RGPIN-2017-04073), Canadian Foundation for Innovation (16659 and 34105), Western Economic Diversification (11270), and King Abdulaziz City for Science and Technology (KACST).

Disclosures. The authors declare no conflicts of interest.

REFERENCES

1. S. Alfihed, J. F. Holzman, and I. G. Foulds, Biosens Bioelectron **165**, 112393 (2020).
2. J. Son, J Appl Phys **105**, 102033 (2009).
3. A. Rahman, A. K. Rahman, and B. Rao, Biosens Bioelectron **82**, 64 (2016).
4. J. F. O'Hara, S. Ekin, W. Choi, and I. Song, Technologies **7**, 43 (2019).
5. N. M. Burford and M. O. El-shenawee, Opt Eng **56**, 010901 (2017).
6. M. Venkatesh, K. S. Rao, T. S. Abhilash, S. P. Tewari, and A. K. Chaudhary, Opt Mater **36**, 596 (2014).
7. V. L. Malevicha, R. Adomavi˘ciusb, and A. Krotkus, C R Phys. **9**, 130 (2008).
8. A. Kumari, A. Chaudhary, and M. Venkatesh, Appl. Opt. **59**, 3417 (2020).
9. C. M. Collier, T. J. Stirling, I. R. Hristovski, J. D. A. Krupa, and J. F. Holzman, Sci Rep **6**, 23185 (2016).
10. J. T. Darrow, X. C. Zhang, D. H. Auston, and J. D. Morse, IEEE J Quantum Electron **28**, 1607 (1992).
11. K. Kitahara, K. Nakai, A. Shibatomi, and S. Ohkawa, Appl Phys Lett **32**, 259 (1978).
12. L. Tian and W. Shi, J Appl Phys **103**, 124512 (2008).
13. J. F. Holzman, P. Strasser, R. Wüest, F. Robin, D. Erni, and H. Jäckel, Nanotechnology **16**, 949 (2005).
14. G. Rodriguez and A. J. Taylor, Opt Lett **14**, 1046 (1996).
15. C. M. Collier, T. J. Stirling, S. Dekock-Kruger, and J. F. Holzman, IEEE J Sel Top Quantum Electron **23**, 8500406 (2017).
16. J. Mareš, J. Krištofik, V. Šmíd, and F. Deml, Solid State Electron **31**, 1309 (1988).
17. J. W. Roach and H. H. Wieder, IEEE Electron Device Lett **6**, 356 (1985).
18. M. Pavlović and U. V. Desnica, Appl Phys Lett **84**, 2018 (1998)
19. A. Singh, S. Pal, H. Surdi, S. S. Prabhu, V. Nanal, and R. G. Pillay, Appl Phys Lett **104**, 063501 (2014).
20. M. R. Stone, M. Naftaly, R. E. Miles, J. R. Fletcher, and D. P. Steenson, IEEE Trans Microw Theory Tech **52**, 2420 (2004).
21. R. Binder, D. Scott, A. E. Paul, M. Lindberg, K. Henneberger, and S. W. Koch, Phys Rev B **45**, 1107 (1992).
22. M. Hase, Appl Phys Lett **94**, 112111 (2009).
23. M. Sotoodeh, A. H. Khalid, and A. A. Rezazadeh, J Appl Phys **87**, 2890 (2000).
24. P. N. Murgatroyd, J Phys D Appl Phys **3**, 151 (1970).

REFERENCES (Full)

1. S. Alfihed, J. F. Holzman, and I. G. Foulds, "Developments in the integration and application of terahertz spectroscopy with microfluidics," Biosens Bioelectron **165**, 112393 (2020).
2. J. Son, "Terahertz electromagnetic interactions with biological matter and their applications," J Appl Phys **105**, 102033 (2009).
3. A. Rahman, A. K. Rahman, and B. Rao, "Early detection of skin cancer via terahertz spectral profiling and 3D imaging," Biosens Bioelectron **82**, 64 (2016).
4. J. F. O'Hara, S. Ekin, W. Choi, and I. Song, "A Perspective on Terahertz Next-Generation Wireless Communications," Technologies **7**, 43 (2019).
5. N. M. Burford and M. O. El-shenawee, "Review of terahertz photoconductive antenna technology," Opt Eng **56**, 010901 (2017).
6. M. Venkatesh, K. S. Rao, T. S. Abhilash, S. P. Tewari, and A. K. Chaudhary, "Optical characterization of GaAs photoconductive antennas for efficient
7. V. L. Malevicha, R. Adomavi˘ciusb, and A. Krotkus, "THz emission from semiconductor surfaces," C R Phys. **9**, 130 (2008).
8. A. Kumari, A. Chaudhary, and M. Venkatesh, "Linear and nonlinear temperature-dependent transmission/absorption characteristics of cadmium telluride crystal for terahertz generation," Appl. Opt. **59**, 3417 (2020).
generation and detection of Terahertz radiation," Opt Mater **36**, 596 (2014).
9. C. M. Collier, T. J. Stirling, I. R. Hristovski, J. D. A. Krupa, and J. F. Holzman, "Photoconductive terahertz generation from textured semiconductor materials," Sci Rep 6, 23185 (2016).
10. J. T. Darrow, X. C. Zhang, D. H. Auston, and J. D. Morse, "Saturation Properties of Large-Aperture Photoconducting Antennas," IEEE J Quantum Electron **28**, 1607 (1992).
11. K. Kitahara, K. Nakai, A. Shibatomi, and S. Ohkawa, "Current-voltage characteristics and deep levels in chromium-doped semi-insulating GaAs," Appl Phys Lett **32**, 259 (1978).
12. L. Tian and W. Shi, "Analysis of operation mechanism of semi-insulating GaAs photoconductive semiconductor switches," J Appl Phys **103**, 124512 (2008).
13. J. F. Holzman, P. Strasser, R. Wüest, F. Robin, D. Erni, and H. Jäckel, "Ultrafast carrier dynamics in InP photonic crystals," Nanotechnology **16**, 949 (2005).
14. G. Rodriguez and A. J. Taylor, "Screening of the bias field in terahertz generation from photoconductors", Opt Lett **14**, 1046 (1996).
15. C. M. Collier, T. J. Stirling, S. Dekock-Kruger, and J. F. Holzman, "Spectral response tuning in photoconductive terahertz emitters with binary phase masks", IEEE J Sel Top Quantum Electron **23**, 8500406 (2017).
16. J. Mareš, J. Krištofik, V. Šmíd, and F. Deml, "On space-charge-limited conduction in semi-insulating GaAs," Solid State Electron **31**, 1309 (1988).
17. J. W. Roach and H. H. Wieder, "Space-charge-limited currents and trapping in semi-insulating InP," IEEE Electron Device Lett **6**, 356 (1985).
18. M. Pavlović and U. V. Desnica, "Precise determination of deep trap signatures and their relative and absolute concentrations in semi-insulating GaAs," Appl Phys Lett **84**, 2018 (1998)
19. A. Singh, S. Pal, H. Surdi, S. S. Prabhu, V. Nanal, and R. G. Pillay, "Highly efficient and electrically robust carbon irradiated semi-insulating GaAs based photoconductive terahertz emitters", Appl Phys Lett **104**, 063501 (2014).
20. M. R. Stone, M. Naftaly, R. E. Miles, J. R. Fletcher, and D. P. Steenson, "Electrical and radiation characteristics of semilarge photoconductive terahertz emitters," IEEE Trans Microw Theory Tech **52**, 2420 (2004).
21. R. Binder, D. Scott, A. E. Paul, M. Lindberg, K. Henneberger, and S. W. Koch, "Carrier-carrier scattering and optical dephasing in highly excited semiconductors," Phys Rev B **45**, 1107 (1992).
22. M. Hase, "Carrier mobility in a polar semiconductor measured by an optical pump-probe technique," Appl Phys Lett **94**, 112111 (2009).
23. M. Sotoodeh, A. H. Khalid, and A. A. Rezazadeh, "Empirical low-field mobility model for III–V compounds applicable in device simulation codes," J Appl Phys **87**, 2890 (2000).
24. P. N. Murgatroyd, "Theory of space-charge-limited current enhanced by Frenkel effect," J Phys D Appl Phys **3**, 151 (1970).